JOURNAL OF THE AMERICAN CHEMICAL SOCIETY
pubs.acs.org/JACS
Article

Selective Cobalt-Mediated Formation of Hydrogen Peroxide from Water under Mild Conditions via Ligand Redox Non-Innocence

Sophie W. Anferov, Jan-Niklas Boyn, David A. Mazziotti, and John S. Anderson*

Cite This: *J. Am. Chem. Soc.* 2024, 146, 5855−5863

Read Online

ACCESS | Metrics & More | Article Recommendations | Supporting Information

ABSTRACT: Despite the broad importance of hydrogen peroxide (H_2O_2) in oxidative transformations, there are comparatively few viable routes for its production. The majority of commercial H_2O_2 is currently produced by the stepwise reduction of dioxygen (O_2) via the anthraquinone process, but direct electrochemical formation from water (H_2O) would have several advantages—namely, avoiding flammable gases or stepwise separations. However, the selective oxidation of H_2O to form H_2O_2 over the thermodynamically favored product of O_2 is a difficult synthetic challenge. Here, we present a molecular H_2O oxidation system with excellent selectivity for H_2O_2 that functions both stoichiometrically and catalytically. We observe high efficiency for electrocatalytic H_2O_2 production at low overpotential with no O_2 observed under any conditions. Mechanistic studies with both calculations and kinetic analyses from isolated intermediates suggest that H_2O_2 formation occurs in a bimolecular fashion via a dinuclear H_2O_2-bridged intermediate with an important role for a redox non-innocent ligand. This system showcases the ability of metal–ligand cooperativity and strategic design of the secondary coordination sphere to promote kinetically and thermodynamically challenging selectivity in oxidative catalysis.

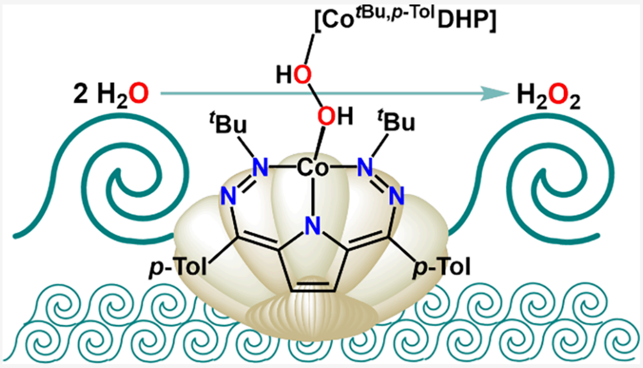

INTRODUCTION

H_2O_2 is an important oxidant that is used on a megaton scale in processes ranging from consumer products to bulk industrial bleaching.[1] The dominant production route for H_2O_2 is the anthraquinone process that uses hydrogen and oxygen gas in a stepwise fashion to generate H_2O_2, a process that also typically incorporates a precious metal catalyst to hydrogenate the quinone. While employed industrially on a large scale, there are several drawbacks to the anthraquinone process including the flammable nature of H_2/O_2,[2] the corresponding requirement for stepwise reactions, as well as the use of currently petroleum-derived H_2. These shortcomings have spurred a great deal of investigation into alternative synthetic routes for H_2O_2 production, with some exciting developments in recent years.[3−5] Still, many of the best catalysts use precious metals, forcing conditions, or require separation between O_2 and H_2 cycling. The use of abundant metal catalysts would be advantageous due to cost and scarcity, but examples using first-row transition metals are limited.[5]

Therefore, interest remains high in discovering alternative H_2O_2 production pathways that are low-cost, nonflammable, highly selective, and simple to operate. Electrocatalysis could fulfill these criteria and has been extensively utilized to take O_2 to H_2O,[6] O_2 to H_2O_2,[7] or H_2O to O_2.[8−11] However, electrocatalysts typically have low selectivity for H_2O oxidation to H_2O_2 as O_2 formation is more exergonic and therefore occurs at milder potentials. In fact, H_2O_2 production is typically viewed as a deleterious side reaction in O_2 evolution electrocatalysis. Precious metals or harsh conditions are still often required in the few reported examples for electrocatalytic H_2O_2 formation from H_2O and mechanistic insights are still limited.[12−14] This is consistent with the fact that H_2O_2 is less favorable to synthesize than O_2, with a thermodynamic potential of 1.76 V compared to 1.23 V vs RHE, respectively.[7b,14b]

We have been interested in using metal–ligand cooperative H atom shuttling to facilitate oxidative and reductive catalysis, particularly within a family of dihydrazonopyrrole (DHP) ligands.[15] We previously observed an unusual homolytic O−H activation of H_2O with the dihydrazonopyrrole complex $(^{Ph,Tol}DHP)Ni$, which resulted in net dihydrogen abstraction and O atom transfer reactivity.[15b] We postulated that this net H atom abstraction from H_2O could be leveraged for a related oxidative catalytic process. There are many examples of Co-

Received: October 6, 2023
Revised: January 30, 2024
Accepted: January 31, 2024
Published: February 20, 2024

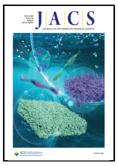

https://doi.org/10.1021/jacs.3c11032

based H_2O oxidation catalysts,[11] and although most systems generate O_2 from H_2O, there are a few reported systems that generate H_2O_2.[14] We also recently reported a DHP Co complex, and we therefore investigated this system for H_2O oxidation reactivity and catalysis.

Here, we report an unusual reaction between water and the previously reported complex $(^{t\text{Bu,Tol}}\text{DHP})\text{CoCl}$ (**1**) to generate the reduced, formally 3-coordinate Co complex $(^{t\text{Bu,Tol}}\text{DHP})\text{Co}$ (**2**) (Scheme 1). Product analysis reveals the formation of H_2O_2 as the byproduct of this reaction, and mechanistic analysis supports a metal–ligand cooperative pathway. This system is competent for electrocatalytic H_2O oxidation to H_2O_2 at low overpotentials with perfect selectivity against O_2 formation. These results show how careful design of the secondary coordination sphere can enable selectivity even for thermodynamically less favorable products in catalysis and provide a proof of concept for direct H_2O to H_2O_2 electrocatalysis.

Scheme 1. $(^{t\text{Bu,Tol}}\text{DHP})\text{CoX}$[15f,h] Reactivity with H_2O

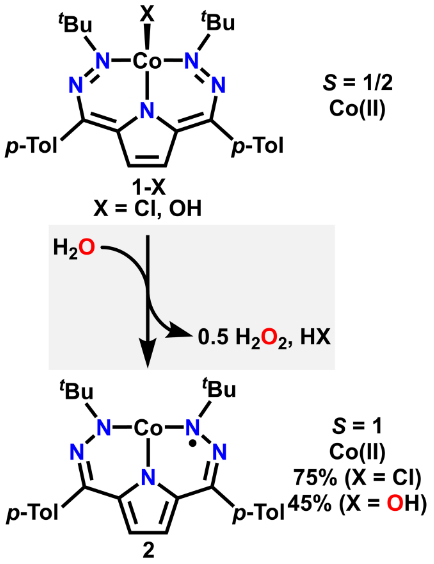

■ RESULTS AND DISCUSSION

Synthesis and Characterization of 2. Given the previously observed reactivity with DHP systems of Ni, we began by investigating the reactivity of **1** with H_2O. Addition of 1 equiv of H_2O to a deep purple solution of $(^{t\text{Bu,Tol}}\text{DHP})\text{CoCl}$ (**1**)[15f] in diethyl ether led to a subtle color change and the isolation of a new compound, $(^{t\text{Bu,Tol}}\text{DHP})\text{Co}$ (**2**), as a purple solid (Scheme 1). This reduced species can also be obtained using more traditional chemical reductants, such as decamethylcobaltacene, as well as from **1-OTf**. This complex is paramagnetic with an $S = 1$ spin state as determined by Evans' method. This spin state suggests either a low-spin $S = 1/2$ Co(II) center ferromagnetically coupled with a $\text{DHP}^{2-\bullet}$ ligand radical, a high spin $S = 3/2$ Co(II) center antiferromagnetically coupled with a $\text{DHP}^{2-\bullet}$ ligand radical, or an intermediate spin $S = 1$ Co(I) center with a diamagnetic DHP^{1-} ligand.

SXRD analysis on dark purple needles of **2** reveals a formally three-coordinate Co center that has a fourth coordinating moiety in the form of an agostic interaction between the Co center and a *tert*-butyl C–H (Figure 1). Using the N1–Co–N5 and N3–Co–(C1–H bond) angles, the τ_4 value for this complex is 0.179 and the τ_4' value is 0.147, putting it closer to square planar than tetrahedral (at 0 and 1, respectively).[16]

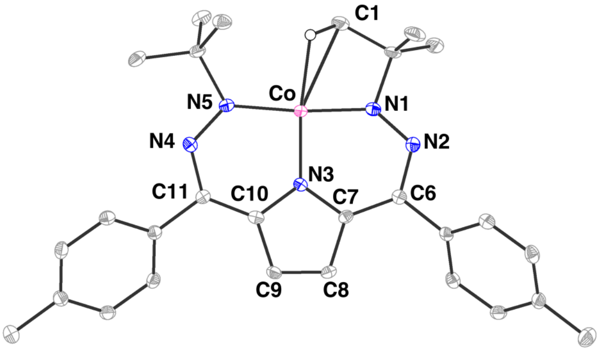

Figure 1. Single-crystal structure of $(^{t\text{Bu,Tol}}\text{DHP})\text{Co}$ (**2**). Selected bond lengths (Å): Co–N1/N5: 1.796(2), 1.847(2); Co–N3: 1.821(2); N1–N2/N4–N5: 1.323(2), 1.318(2); Co–(C1–H): 1.770(2); N2–C5/N4–C10: 1.343(3), 1.336(3); C5–C6/C9–C10: 1.403(3), 1.402(3); C6–C7/C8–C9: 1.436(3), 1.433(3); C7–C8: 1.353(3). Selected bond angles (deg): N1–Co–N5: 172.33(8); N3–Co–(C1–H): 162.15(8).

The Co–(C1–H) interaction is best described as agostic, not anagostic, as the distance between Co and the H of the interacting C–H bond, which can be resolved in the difference map, is 1.89(2) Å, within the ~1.8–2.3 Å range for an agostic bond vs anagostic bonds, which are typically longer.[17] The Co–H–C1 angle is 110.1(2)°, also well within the acceptable range for an agostic interaction. While ^{1}H NMR is frequently also used as a diagnostic for agostic interactions, the paramagnetic state of **2** prevents its use here.

Comparison of the bond lengths in **2** with the previously reported structures of **1**, $(^{t\text{Bu,Tol}}\text{DHP})\text{CoOH}$ (**1-OH**), and related DHP complexes of Ni provides more insight on the formal electronic structure of this newly synthesized compound. We have found that redox changes on the DHP ligand result in diagnostic changes to specific bonds, namely, N1–N2/N4–N5, C5–C6/C9–C10, and C7–C8. Comparison of these distances between **2** and **1**, **1-OH**, and the Ni complexes $(^{\text{Ph,Tol}}\text{DHP})\text{NiPMe}_3{}^{n+}$ ($n = 0$ and 1)[15a] suggests that the DHP ligand in **2** is best considered as a dianionic $\text{DHP}^{2-\bullet}$ unit, implying a high-spin Co(II) center. DFT calculations on **2** support this electronic structure assignment. A calculated spin density plot of a PBE0/def2-TZVP optimized structure of **2** most distinctly resembles a high spin Co(II) with an antiferromagnetically coupled ligand radical (Figure S54). However, these are highly covalent systems and concrete assignments of oxidation states are difficult. This electronic structure description is also consistent with previously isolated examples of antiferromagnetically coupled compounds with this ligand framework.[15a,15]

Stoichiometric Hydrogen Peroxide Production from Water. The yield of **2** from the reaction of **1** with H_2O is high (75%), which raises the question of the oxidized product to balance the formal reduction from $[(\text{DHP}^{2-\bullet})\text{Co(II)}]^+$ to $[(\text{DHP}^-)\text{Co(II)}]$. We additionally investigated whether other X-type ligands bound to Co would also serve as suitable synthons for the formation of **2**, and we indeed observe that addition of H_2O to the Co–OH complex (**1-OH**) also forms **2**, albeit in lower yield (45(5)%). The DHP ligand is formally reduced by one electron in both of these reactions, presumably by H_2O. This suggests that water oxidation byproducts might be likely candidates to balance this reaction, and the literature

Scheme 2. Proposed Mechanism for the Molecular and Catalytic Generation of H_2O_2 from the Reaction between Co(^{tBu,Tol}DHP) Complexes and H_2O[a]

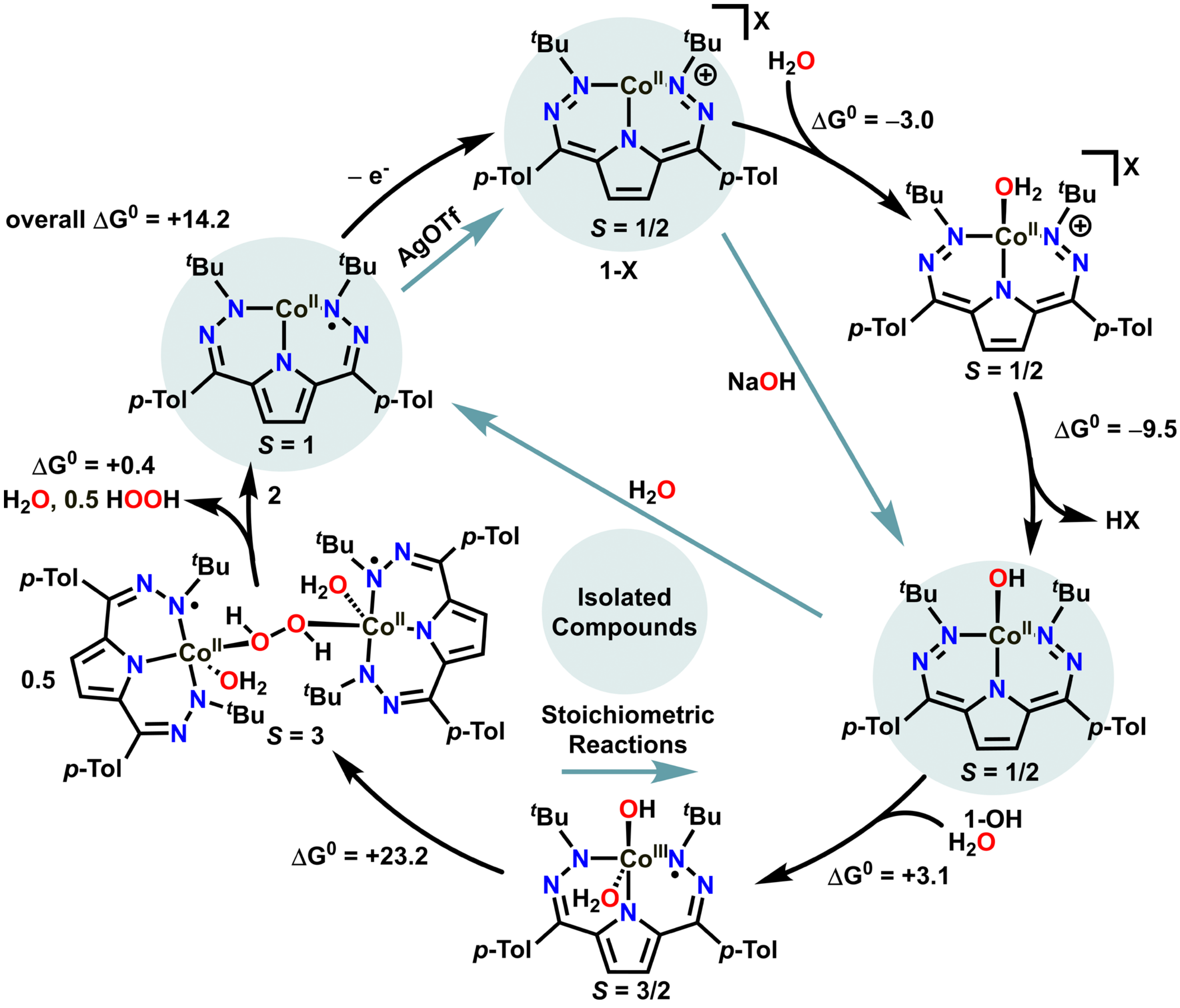

[a] All energies shown in kcal/mol.

precedent for Co-catalyzed O_2 evolution from H_2O led us to test for this product as a likely candidate. Surprisingly, no O_2 has been detected from these reactions via GC under any conditions, which required the consideration of alternative products, one of which could be H_2O_2.

We therefore employed a H_2O_2-specific organic probe, 1,3-diphenylisobenzofuran.[18] This organic probe has been shown to only produce 9-hydroxyanthracen-10(9*H*)-one in the presence of H_2O_2 (and not other oxidants), while 1,2-dibenzoylbenzene can be formed from H_2O_2 and many other oxidants. The presence of 9-hydroxyanthracen-10(9*H*)-one after reacting **1** or **1-OH** with H_2O in the presence of 1,3-diphenylisobenzofuran would therefore strongly indicate H_2O_2 production. Indeed, GCMS analysis of the reaction of **1** and H_2O in the presence of 1,3-diphenylisobenzofuran reveals a 10.2% yield of the H_2O_2-diagnostic product, 9-hydroxyanthracen-10(9*H*)-one, and a 4.4% yield of 1,2-dibenzoylbenzene as another oxidation product (Figures S69−S71). While the presence of 9-hydroxyanthracen-10(9*H*)-one is conclusively indicative of H_2O_2 formation, 1,2-dibenzoylbenzene is an intermediate oxidation product formed from 1,3-diphenylisobenzylfuran. Given that this probe usually incompletely captures formed H_2O_2,[18] this sets a lower bound of 20.4% yield for H_2O_2 production (since 2 equiv is necessary to form the diagnostic product) and a lower bound of 24.8% yield for total oxidized product production from **1**.

In addition to 1,3-diphenylisobenzofuran, we can also use alternative oxidant probes such as triphenylphosphine or iodide to quantify the amount of oxidized products. Reacting **1** with 1 equiv of H_2O in the presence of 1 equiv of PPh_3 gave 33% yield of the oxidized phosphine (Figures S72 and S73). H_2O_2 can be quantified from the reaction from **1** to **2** via an iodide assay, with a yield of 44(4)% of I_3^-, supporting the expected 0.5 equiv of H_2O_2 being formed. These observations strongly support H_2O_2 as a product of these reactions, and they also suggest that a balanced reaction of **1** + H_2O → **2** + HCl + $0.5H_2O_2$ is plausible.

Mechanistic Interrogation. We then wanted to understand a possible mechanism of this unusual transformation. Complex **1-OH** had been previously characterized, and we postulated that it might be a reasonable intermediate formed via H_2O binding and deprotonation. However, the crucial step to form H_2O_2 remained less clear, so we used density functional theory (DFT) calculations to evaluate possible mechanisms. After investigating several possible pathways via single-point energy calculations with O3LYP (Scheme 2 and Figures S50−S52), the most energetically accessible mechanism is calculated to go first through acid elimination and then through a dimeric intermediate that releases H_2O_2. Utilizing PBE0 and with entropy contributions, we calculate that the first half of the mechanism to form **1-OH** from $\mathbf{1}^+$ is exergonic, with an initial favorable binding of water of −3.0 kcal/mol, followed by acid elimination that is favorable by −9.5 kcal/mol to form **3**. Subsequent H_2O binding is accessible and only slightly disfavored (endergonic by 3.1 kcal/mol).

Complex **1-OH** is an isolable low-spin $S = 1/2$ species. However, DFT calculations predict that binding of a fifth ligand leads to an $S = 3/2$ intermediate. While the low-spin (LS) state of **1-OH** is 17.9 kcal/mol below the high-spin (HS) state, with the addition of water, the HS state of **1-OH**-H_2O becomes significantly lower (by 17.9 kcal/mol). Spin density plots reveal that more spin is delocalized onto the DHP and OH ligands in the HS analogs, as expected (Figures S58 and S59). Tautomerism calculations using different broken-symmetry fragment-guess wave functions in DFT echo this result—with addition of the H_2O ligand significantly increasing Mulliken charge on Co, flipping the preference for Co^{III} over Co^{II} and increasing delocalization of the unpaired spin density (Figures S67 and S68). This fifth ligand coordination is key to the predicted formation of the dimer, as calculations of subsequent steps that do not include a fifth ligand are not predicted to yield stable structures. Experimentally, we note that addition of an additional ligand is not limited to H_2O, as addition of acetonitrile to **1-OH** also promotes the formation of **2** and H_2O_2 (Figure S4). These analyses underscore the importance of the spin- and oxidation-state change induced by ligand coordination in helping to drive H_2O_2 formation and echo previous observations of valence tautomerism in heme systems.[19]

The predicted rate-determining step is the formation of the H_2O_2-bridged dimer, which is uphill by 23.2 kcal/mol from **1-OH**-H_2O. As mentioned, we observe increased electron density on the −OH ligand in the putative 5-coordinate intermediate **1-OH**-H_2O and it is possible that this increased radical character facilitates the subsequent dimerization step. Release of H_2O_2 and H_2O and production of **2** are nearly thermoneutral at only 0.4 kcal/mol endergonic.

Within this mechanism, **1**, **2**, and **1-OH** are all synthetically accessible, which provides several avenues to perform mechanistic experiments (Scheme 2). The DFT-predicted rate-determining step suggests that a second-order process might be expected from kinetic analyses. We therefore used UV−vis analysis to monitor the addition of either H_2O or an exogenous ligand (acetonitrile) to **1-OH** under pseudo-first-order conditions. This analysis reveals consecutive isosbestic transformations (Figure 2A,B). The first transformation is rapid and first-order. We interpret this conversion as a ligand binding event (Scheme 2). A slower, second-order transformation is then observed (Figure 2B).

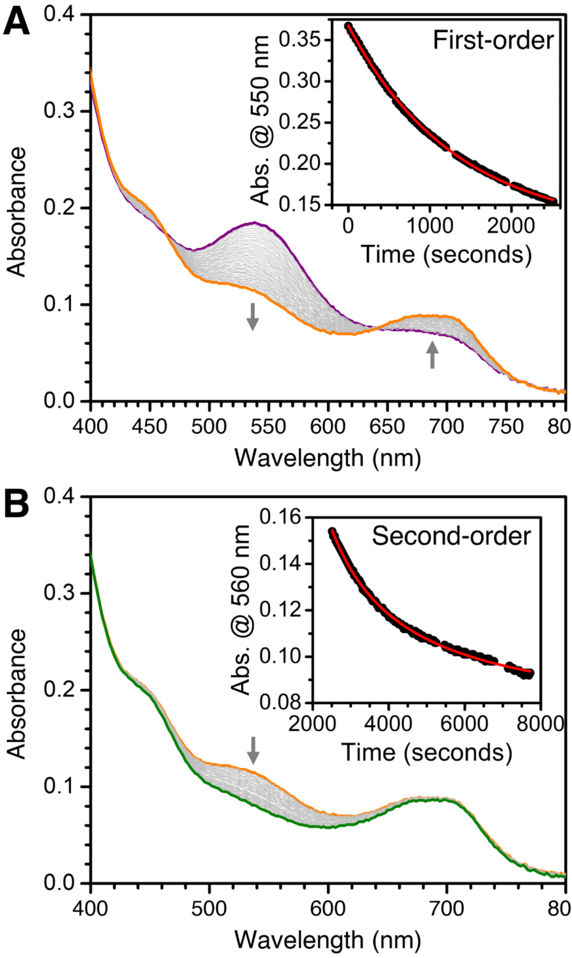

Figure 2. UV−vis analysis of 0.094 mM **1-OH** reacting with acetonitrile under pseudo-first-order conditions in diethyl ether at 2 °C. (A) Traces taken during the first 2500 s of the reaction, with an inset showing a first-order fit to the absorbance at 560 nm. (B) Traces taken from 2500 to 7700 s, with an inset showing a second-order fit to the absorbance at 560 nm. Details on fitting and parameters are provided in the Supporting Information.

We then used an Eyring analysis to test whether the observed rates were qualitatively consistent with the barriers predicted from DFT. We note that slightly different values between experiment and DFT are expected due to the use of acetonitrile instead of H_2O as our added ligand in our kinetic measurements for experimental ease. We find that $\Delta H^{\ddagger}$ = 11.4(3) kcal/mol and $\Delta S^{\ddagger}$ = −28(1) cal/(mol·K) for the second-order process. These values provide 22 °C $\Delta G^{\ddagger}$ = 19.8(3) kcal/mol, in good agreement with the DFT-predicted barrier for this process. Furthermore, the negative entropy of activation also supports dimerization.

The DFT calculations above suggest a dimerization pathway, and we therefore assign this second-order process to that step. These measurements were done in triplicate to ensure fidelity, and both first-order and second-order fits are done via an Espenson treatment (Figures S12−S18).[20] The complicated feature observed around 700 nm is also consistent with the major feature in the DFT-predicted spectrum of such a dimeric species (Figures S48 and S49). The transformation is not isosbestic at longer time points, likely due to degradation that occurs as H_2O_2 is released from the dimer. We note that H_2O_2

reacts with the starting complex and the intermediates that we can isolate, consistent with this hypothesis.

The DFT calculations predict an endergonic conversion of **1-X** to **2**, even though we observe this reaction to be spontaneous with added H_2O or MeCN (Figure S4). While the accuracy of the energetics from DFT is likely limited due to the complicated electronic structure of this putative dimeric intermediate, we also propose that oxidative complex or solvent degradation from formed H_2O_2 or acid helps drive this reaction. Notably, inclusion of a mild base (2,6-lutidine) or a H_2O_2 trap (NaI) makes the overall reaction exergonic (Figure S66 and Table S9). This computational prediction is also supported experimentally. Reaction of **1-Cl** with H_2O in a biphasic reaction in the presence of both 2,6-lutidine and NaI allows for the characterization of the stoichiometry of this reaction. ^1H NMR quantification with an internal standard reveals a 78% yield of ^{tBu,Tol}DHPCo(MeCN) (**2-MeCN**) and an 89% yield of [2,6-lutidinium][Cl]. Concomitant quantification of NaI_3 shows an 80% yield of the expected half-equivalent formed (Figure S3). The observations of high yields of both the protonated base and oxidation of the added H_2O_2 trap support both the proposed stoichiometry and the role of the sacrificial base/reductant in this process.

It is less clear what the sacrificial base/reductant is in reactions without added reagents, i.e., the direct reaction between **1-X** or **1-OH** and H_2O or MeCN. We hypothesize that some amount of the starting DHP Co complex serves in this role, consistent with the substoichiometric yields of **2** that are observed. Indeed, oxidized ligand products are observed in GCMS following the crude reaction from **1-OH** to **2** that are not observed in the GCMS of either isolated complex (Figures S74 and S75). We note literature precedent that acetonitrile and H_2O_2 mixtures can form peroxyacetimidic acid in equilibrium, which is then capable of oxidizing tertiary amines.[21] Finally, the IR spectrum of crude freshly formed **2** shows a number of low-intensity N−H stretches, consistent with protonated DHP fragments serving a sacrificial role in this reaction (Figures S20 and S21).

All of these observations suggest that an overall endergonic process to generate H_2O_2 predicted from DFT calculations is likely driven by H_2O_2 consumption from various oxidative decomposition pathways. While this mechanistic proposal is tentative due to the complexity of the system, all computational and experimental data obtained thus far support this general pathway. Despite convolutions from mechanistic complexity and decomposition pathways, the generation of **2**, which can be stoichiometrically oxidized back to **1-OTf**, suggests that a catalytic cycle should be possible.

Catalytic Hydrogen Peroxide Production from Water.

We initially wanted to examine the feasibility of catalysis using chemical oxidants. Addition of H_2O and AgOTf in acetonitrile to 5 mol % **2** results in the growth of a new ^1H NMR peak at 8.6 ppm (Figure S6), where H_2O_2 appears in MeCN, providing direct evidence for the presence of H_2O_2.[22] Integration of this ^1H NMR spectrum reveals that ∼50% of the H_2O peak is consumed and that ∼5.5 equiv of H_2O_2 per Co center is formed. Unassigned organic peaks are also observed, which suggests some degree of ligand decomposition, consistent with our previous results suggesting that ligand oxidation is occurring and potentially helping drive H_2O_2 formation. These results support catalytic water oxidation to H_2O_2 mediated by **2**. However, we also wanted to corroborate this observation via an orthogonal technique, namely, with electrochemistry.

Complex **2** displays four distinct redox waves in its cyclic voltammogram (CV) in THF (Figure S24). This is similar to the CV of **1** in THF with some small shifts likely derived from differences in counteranions.[15f,h] This electrochemical data exhibits the unusually rich redox-flexibility characteristic of the ^{tBu,Tol}DHP scaffold. Acetonitrile, which is the most tractable solvent for electrochemical studies, significantly complicates the voltammogram by adding new features and making some previous features irreversible, putatively due to solvent coordination (Figure S23). With the addition of H_2O and a mild base, in the form of 2,6-lutidine, catalytic current enhancement can be observed in the CV (Figure 3A). The oxidative feature at 0.85 V before the onset of catalysis can likely be assigned to the first oxidation of the acetonitrile or water adduct of **2**. The shape of the catalytic wave is complex even at varying scan rates, making detailed interpretation, for instance, with foot-of-the-wave analysis, difficult (Figure S30).[23] **1**, **1-OTf**, and **2** all display similar electrocatalytic features under similar conditions (Figures S27−S29). In acetonitrile, the thermodynamic potential for H_2O oxidation to H_2O_2 in the presence of 2,6-lutidine is 0.944 V vs Fc/Fc$^+$ and, while a precise value for overpotential is difficult to ascertain due to the complicated CV waveform, our observed

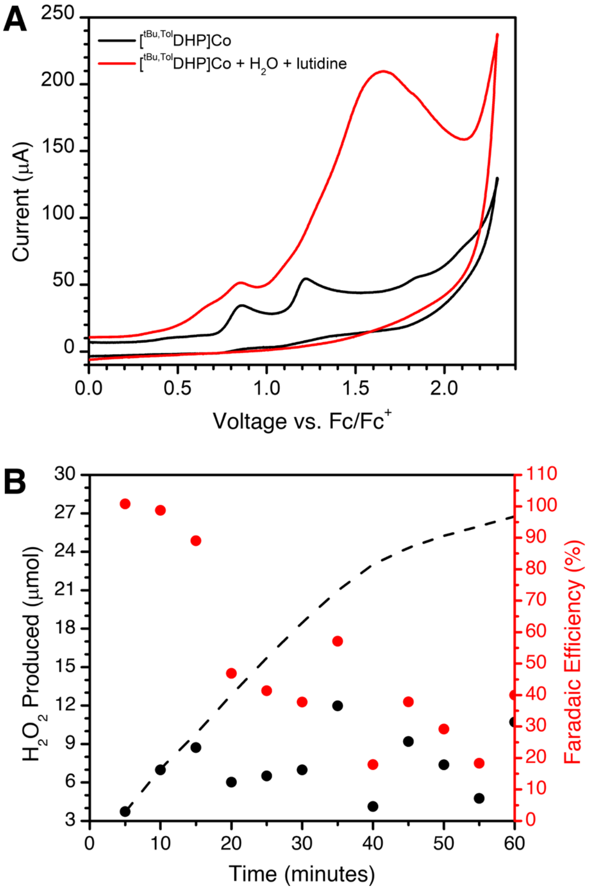

Figure 3. (A) Current enhancement observed in the presence of **1**, H_2O, and 2,6-lutidine (1 mM **1**, 320 mM H_2O, and 160 mM 2,6-lutidine in acetonitrile with 0.1 M NBu_4PF_6). (B) Theoretical yield (black) and experimental yield (red) determined via NaI assay in micromoles of H_2O_2 plotted against time (seconds).

catalytic onset is clearly just above this thermodynamic value (eq S4).

We performed H_2O_2 quantification to determine the Faradaic efficiency for this product (Figure 3). Unlike our chemical reactions above, we can quantify with NaI assays for these electrochemical reactions.[24] When monitored over time, we observe an average 41% Faradaic efficiency for H_2O_2 production over 60 min, with notably higher values (>90%) at early time points. Furthermore, we see the net amount of detected H_2O_2 plateau after ∼30 min (Figure 3B). We attribute both of these observations to the side reaction of H_2O_2 with the catalyst or the electrolyte solution over time. Over 60 min, 13 C of current is passed, which corresponds to 10 e^- per Co and a TON of 5, assuming 100% Faradaic efficiency for H_2O_2 or 2.2 if the average Faradaic efficiency is used. These TONs are highly reproducible, and an average TON of 6(2) was obtained over 8 individual runs.

Evidence for the instability of **1** in the presence of excess H_2O_2 can be confirmed by CVs taken in the presence of **1**, 2,6-lutidine, and varied amounts of $H_2O_2 \cdot 2OPPh_3$. Although robust with 1 equiv of $H_2O_2 \cdot 2OPPh_3$, the voltammogram of this solution begins to change with 10 or more equivalents of this H_2O_2 surrogate and shows significant changes after 20 equiv, consistent with the decomposition of **1** after sufficient H_2O_2 production (Figure S36).

Importantly, no O_2 has been detected via GC from any experimental setup, supporting the fact that H_2O_2 is the sole product of electrocatalysis (Figure S76). The observed decrease in current and Faradaic efficiency argues against some decomposed product mediating catalysis such as an oxide. However, we also obtained further experimental evidence against the agency of any solid-state catalysts. Removal of the electrode after bulk electrolysis and subsequent analysis by CV shows no catalytic current (Figure S26). Furthermore, SEM/EDS analysis on the electrode after bulk electrolysis also shows no evidence for the formation of CoO_x materials (Figures S77 and S78).[25] Additionally, a control using solely $CoCl_2$ generates only O_2 as a product of electrocatalysis under analogous conditions (Figure S34). We note that some CoO_x materials are competent for the more unusual production of H_2O_2, but this is more typically observed under acidic conditions.[26] All of these combined observations support a molecular catalyst for the observed H_2O_2 formation.

■ CONCLUSIONS

Here, we present a molecular system that selectively produces H_2O_2 stoichiometrically and catalytically. Calculations, isolable intermediates, and kinetic analyses suggest that H_2O_2 formation proceeds through dimerization to form a H_2O_2-bridged dimeric intermediate. This overall pathway is facilitated by the redox activity of the dihydrazonopyrrole ligand scaffold on this system.

It is worth noting that H_2O_2 is the only observed product in these reactions, with no generation of O_2 despite the thermodynamic preference for this product. High selectivity for H_2O_2 over O_2 is unusual in homogeneous electrocatalysts. Related catalytic systems that electrochemically generate H_2O_2 from H_2O show Faradaic efficiencies that range broadly between 15 and 85%, with significant current fractions going to O_2 production or even other side reactions.[12−14] High Faradaic efficiency for H_2O_2 in the absence of concurrent O_2 production is quite rare. Co corrole systems are among the best H_2O to H_2O_2 electrocatalysts, but even these examples have imperfect selectivity with ∼20% or more of the Faradaic efficiency going to O_2.[14]

A further unique feature of the present system is its proposed mechanism. Other homogeneous electrocatalysts, including the aforementioned corrole systems, either do not make mechanistic proposals or invoke the activity of free hydroxyl radicals or OH^- attack on a reactive oxo/hydroxo-species.[12−14] The mechanistic experiments provided here by both DFT and UV−vis monitoring suggest a comparatively unique bimetallic pathway. The observed stoichiometric reactivity is also unusual; molecular complexes that directly generate H_2O_2 from H_2O without an added oxidant are rare. While the low stability of the current system limits its catalytic utility, these results do demonstrate how molecular design principles can enable selectivity for thermodynamically more difficult products, further underscoring how metal−ligand cooperativity can enable new reactivity and catalysis.

■ EXPERIMENTAL SECTION

General Methods. All chemicals were purchased from commercial suppliers and used without further purification. All manipulations were carried out under an atmosphere of N_2 using standard Schlenk and glovebox techniques. Glassware was dried at 180 °C for a minimum of 2 h and cooled under vacuum prior to use. Solvents were dried on a solvent purification system from Pure Process Technologies and stored over 4 Å molecular sieves under N_2. Tetrahydrofuran (THF) was stirred over NaK alloy and run through an additional alumina column prior to use to ensure dryness. Solvents were tested for H_2O and O_2 using a standard solution of sodium-benzophenone ketyl radical anion. CD_3CN, C_6D_6, and d_8-toluene were dried over 4 Å molecular sieves under N_2.

^1H and ^{19}F NMR spectra were recorded on Bruker DRX 400 or 500 spectrometers. Chemical shifts are reported in ppm units referenced to residual solvent resonances for ^1H and $^{31}H\{^1H\}$ spectra. UV−visible spectra were recorded on a Bruker Evolution 300 spectrometer and analyzed using VisionPro software. A standard 1 cm quartz cuvette with an airtight screw cap with a puncturable Teflon seal was used for all measurements. A Unisoku CoolSpek cryostat was used for low-temperature measurements. ^1H and ^{19}F NMR spectra were recorded on either Bruker DRX-400 or AVANCE-500 spectrometers. IR spectra were recorded on either a Bruker Tensor II spectrometer with the OPUS software suite as DCM thin films between KBr plates or a Bruker α II spectrometer in a nitrogen, dry glovebox with the OPUS software suite as diethyl ether thin films on a Platinum Diamond ATR module. Single-crystal X-ray diffraction data were collected in-house using a Bruker D8 Venture diffractometer equipped with a Mo microfocus X-ray tube (λ = 0.71073 Å). Combustion analysis was performed by Midwest Microlab. Electrochemical measurements were carried out using a BAS Epsilon potentiostat and using BAS Epsilon software version 1.40.67 NT. Magnetic moments were determined using the Evans method.[27]

Electrochemical Experiments. Experiments were performed inside the glovebox with a MeCN/0.1 M NBu_4NPF_6 electrolyte solution at room temperature. Cyclic voltammetry measurements were made with [**Co**] = 1 mM using a glassy carbon working electrode, platinum wire counter electrode, and silver wire pseudoreference electrode and were referenced to internal Fc/Fc^+ by adding ferrocene at the end of the measurements. A one-compartment glass cell was filled with 4 mL of electrolyte solution. The working electrode was polished over a microcloth pad (Buehler) using alumina slurry (0.05 mm EMS), followed by rinsing with deionized water and isopropyl alcohol. Reference and counter electrodes were rinsed with acetone. CVs were recorded at a scan rate of 200 mV/s scanning oxidatively.

Electrolyses were performed in a sealed H-type glass cell with anode and cathode chambers separated by a glass frit. A graphite rod electrode, Pt-mesh electrode, and silver wire pseudoreference electrode were used as working, counter, and reference electrodes, respectively. To each chamber of the H-cell were added a 10 mL electrolyte solution and stir bars. Typically, 5.4 mg of (DHP)CoCl (final concentration, 1 mM), 160 equiv of 2,6-lutidine, and 320 equiv of H_2O were added to the cathodic chamber. H_2O (320 equiv) was also added to the anodic chamber. Post electrolysis, the sealed atmosphere was sampled with a gastight syringe and analyzed by GC for O_2.

$(^{tBu,Tol}$DHP)Co (2). In a 20 mL vial in the glovebox, 1−2 mL of diethyl ether was added until $(^{tBu,Tol}$DHP)CoCl (**1**, 15.0 mg, 0.028 mmol)[15f] dissolved completely to generate a purple solution. A concentrated solution of 10 μL of H_2O or D_2O in 1 mL of diethyl ether was prepared. From this stock solution, a 3 μL aliquot was taken (1 equiv, 0.028 mmol) and added to the solution of **1**. The solution remained purple and was allowed to react for 1 h. After this time, the solution was dried *in vacuo* and the remaining solids were extracted with petroleum ether. This petroleum ether fraction could be filtered and dried *in vacuo* to obtain crude **2** in 75% yield (0.0105 g, 0.0210 mmol). This crude solid can be recrystallized out of concentrated petroleum ether. We note that additional crops of material can be obtained by benzene extraction of any remaining solids. Single crystals for XRD were grown by cooling a diethyl ether solution of this product at −35 °C. We note that similar procedures with alternative bound anions (i.e., OTf^- or OH^-) also provide **2**, albeit in slightly lower yield (45(5)%, 0.0063 g, 0.126 mmol, for X = OH). ^1H NMR (400 MHz, C_7D_8, RT): δ = 7.47 (br s), 2.72 (br s). Magnetic susceptibility: Evans' method (C_6D_6, RT, μ_B): μ_{eff} = 2.90; UV−vis, nm in diethyl ether (ε, M^{-1} cm^{-1}): 4342.64. HRMS (EI) *m*/*z*: $[M]^+$ calculated for **1**: $C_{28}H_{34}N_5Co$, 499.2121; found, 499.2164.

Reoxidation of $(^{tBu,Tol}$DHP)Co (2) to $(^{tBu,Tol}$DHP)CoOTf (1-OTf). In a 20 mL vial in the glovebox, 2 mL of acetonitrile was added to $(^{tBu,Tol}$DHP)Co (0.002 g, 1 equiv, 0.0039 mmol). A solution of silver triflate (0.001g, 1 equiv, 0.0039 mmol) in acetonitrile was added dropwise, resulting in a color change from brown/purple to dark green. This was stirred for 30−60 min and subsequently dried *in vacuo* to a dark maroon solid, which could then be collected into benzene. Yield: 0.0024 g, 92%. The NMR was found to match the previously reported NMR for **5**.[15f] This reaction could also be followed by NMR and seemed to have quantitative yields with no overoxidation occurring.

Biphasic Reaction of $(^{tBu,Tol}$DHP)CoCl (1) to $(^{tBu,Tol}$DHP)Co-(MeCN) (2-MeCN). In a 20 mL vial in the glovebox, 2 mL of diethyl ether was added to $(^{tBu,Tol}$DHP)CoCl (**1**) (0.0011 g, 1 equiv, 0.0020 mmol). A solution of sodium iodide (0.003 g, 10 equiv, 0.0200 mmol) in H_2O was added, and the resulting solution was stirred for 30 min. The diethyl ether solution was pipetted off and subsequently dried *in vacuo* to a dark purple solid. This solid was dissolved in CD_3CN, and the yield of NaI_3 in the H_2O fraction was quantified by UV−vis analysis. Yield of **2-MeCN**: 0.0008 g, 78%; yield of NaI_3: 40% (relative to **1**); yield of 2,6-lutidinium chloride: 89%. The NMR was found to match that previously reported for **2-MeCN**.

Preparation of UV−vis Samples for H_2O_2 Quantification via I_3^-. *Postbulk Electrolysis.* The remaining acetonitrile solution from bulk electrolysis was placed into a vial with excess NaI and stirred over 4−5 h before drying *in vacuo*. The solids were washed with toluene to remove organic products and then extracted into acetonitrile or water. An aliquot was measured by a syringe and transferred into a cuvette for UV−vis analysis. For larger runs, a volumetric flask was used to measure volume, and a known amount was transferred into the cuvette by a syringe. The extinction coefficient of I_3^- does not vary significantly between acetonitrile and water, but nevertheless, we made sure that water was always present in excess to maintain consistency.[28]

Molecular Reactions. The procedure above for the synthesis of **2** was altered in the following fashion to obtain yields with NaI (5−10 equiv). **1** (2 mg, 0.0037 mmol) was dissolved in 50 μL of dichloromethane, and a NaI (5 equiv) solution in 2.5 mL of H_2O was added to this solution. The biphasic mixture was stirred for 30 min, and then the I_3^- content of the H_2O layer was quantified by UV−vis analysis.

■ ASSOCIATED CONTENT

Supporting Information

The Supporting Information is available free of charge at https://pubs.acs.org/doi/10.1021/jacs.3c11032.

Experimental procedures and NMR, IR, GC-MS, CV, UV−vis, SXRD, and DFT data (PDF)

Combined *xyz* datasets (ZIP)

Accession Codes

CCDC 2298058 contains the supplementary crystallographic data for this paper. These data can be obtained free of charge via www.ccdc.cam.ac.uk/data_request/cif, or by emailing data_request@ccdc.cam.ac.uk, or by contacting The Cambridge Crystallographic Data Centre, 12 Union Road, Cambridge CB2 1EZ, UK; fax: +44 1223 336033.

■ AUTHOR INFORMATION

Corresponding Author

John S. Anderson − *Department of Chemistry, The University of Chicago, Chicago, Illinois 60627, United States;* orcid.org/0000-0002-0730-3018; Email: jsanderson@uchicago.edu

Authors

Sophie W. Anferov − *Department of Chemistry, The University of Chicago, Chicago, Illinois 60627, United States;* orcid.org/0000-0003-3972-5845

Jan-Niklas Boyn − *Department of Mechanical and Aerospace Engineering, Princeton University, Princeton, New Jersey 08544, United States;* orcid.org/0000-0002-6240-3759

David A. Mazziotti − *Department of Chemistry, The University of Chicago, Chicago, Illinois 60627, United States;* orcid.org/0000-0002-9938-3886

Complete contact information is available at: https://pubs.acs.org/10.1021/jacs.3c11032

Author Contributions

All authors have given approval to the final version of the manuscript.

Notes

The authors declare no competing financial interest.

■ ACKNOWLEDGMENTS

This work was supported by the National Institutes of Health (R35GM133470). We thank the University of Chicago for funding, the 3M Corporation for an NFTA to J.S.A., and the Sloan Foundation for a Research Fellowship to J.S.A. (FG-2019-11497). D.A.M. gratefully acknowledges the U.S. National Science Foundation Grant No. CHE-2155082 and the U.S. Department of Energy, Office of Basic Energy Sciences, Grant DE-SC0019215.. We also thank the Research Computing Center at the University of Chicago for providing computing resources. This work made use of the shared facilities at the University of Chicago Materials Research Science and Engineering Center (MRSEC), supported by the National Science Foundation under award number DMR-2011854. We would like to thank A. Anferov for assistance with the collection and processing of SEM and EDS data, as well as for valuable experimental input. We would also like to thank Drs. C. McCrory, P. Verma, K. Jesse, S.J., and M.W. for helpful discussions.

REFERENCES

(1) (a) Jones, C. W.; Clark, J. H. In *Applications of Hydrogen Peroxide and Derivatives*, Jones, C. W., Ed.; Royal Society of Chemistry: Cambridge, U.K., 1999; 1− 35. (b) Eul, W.; Moeller, A.; Steiner, N. Hydrogen peroxide. In *Kirk-Othmer Encyclopedia of Chemical Technology*; Wiley, 2001. (c) Campos-Martin, J. M.; Blanco-Brieva, G.; Fierro, J. L. G. Hydrogen Peroxide Synthesis: An Outlook beyond the Anthraquinone Process. *Angew. Chem., Int. Ed.* **2006**, *45*, 6962. (d) Chen, Q. Development of an Anthraquinone Process for the Production of Hydrogen Peroxide in a Trickle Bed Reactor-From Bench Scale to Industrial Scale. *Chem. Eng. Process.* **2008**, *47*, 787−792. (e) Lewis, R. J.; Hutchings, G. J. Recent Advances in the Direct Synthesis of H_2O_2. *ChemCatChem.* **2019**, *11*, 298.

(2) Schröder, V.; Emonts, B.; Janßen, H.; Schulze, H.-P. Explosion Limits of Hydrogen/Oxygen Mixtures at Initial Pressures up to 200 bar. *Chem. Eng. Technol.* **2004**, *27*, 847.

(3) (a) Choudhary, V. R.; Gaikwad, A. G.; Sansare, S. D. Nonhazardous Direct Oxidation of Hydrogen to Hydrogen Peroxide Using a Novel Membrane Catalyst. *Angew. Chem., Int. Ed.* **2001**, *40*, 1776. (b) Edwards, J. K.; Solsona, B.; Ntainjua, E. N.; Carley, A. F.; Herzing, A. A.; Kiely, C. J.; Hutchings, G. J. Switching Off Hydrogen Peroxide Hydrogenation in the Direct Synthesis Process. *Science* **2009**, *323*, 1037. (c) Edwards, J. K.; Freakley, S. J.; Carley, A. F.; Kiely, C. J.; Hutchings, G. J. Strategies for Designing Supported Gold−Palladium Bimetallic Catalysts for the Direct Synthesis of Hydrogen Peroxide. *Acc. Chem. Res.* **2014**, *47*, 845. (d) Freakley, S. J.; He, Q.; Harrhy, J. H.; Lu, L.; Crole, D. A.; Morgan, D. J.; Ntainjua, E. N.; Edwards, J. K.; Carley, A. F.; Borisevich, A. Y.; Kiely, C. J.; Hutchings, G. J. Palladium-tin catalysts for the direct synthesis of H_2O_2 with high selectivity. *Science* **2016**, *351*, 965. (e) Wilson, N. M.; Flaherty, D. W. Mechanism for the direct synthesis of H2O2 on Pd clusters: heterolytic reaction pathways at the liquid−solid interface. *J. Am. Chem. Soc.* **2016**, *138*, 574. (f) Shi, X.; Siahrostami, S.; Li, G.-L.; Zhang, Y.; Shakthranont, P.; Studt, F.; Jaramillo, T. F.; Zheng, X.; Norskov, J. K. Understanding activity trends in electrochemical water oxidation to form hydrogen peroxide. *Nat. Comm.* **2017**, *8*, 701. (g) Liu, J.; Zou, Y.; Jin, B.; Zhang, K.; Park, J. H. Hydrogen Peroxide Production from Solar Water Oxidation. *ACS Energy Lett.* **2019**, *4* (12), 3018.

(4) (a) Gamage, S. N.; James, B. R. Catalytic Formation of an Amide Hydroperoxide and Hydrogen Peroxide using Rhodium Complexes and Dioxygen/Dihydrogen Mixtures. *J. Chem. Soc., Chem. Commun.* **1989**, 1624. (b) Shibata, S.; Suenobu, T.; Fukuzumi, S. Direct Synthesis of Hydrogen Peroxide from Hydrogen and Oxygen by Using a Water-Soluble Iridium Complex and Flavin Mononucleotide. *Angew. Chem., Int. Ed.* **2013**, *52*, 12327. (c) Ogo, S.; Yatabe, T.; Tome, T.; Takenaka, R.; Shiota, Y.; Kato, K. Safe, One-Pot, Homogeneous Direct Synthesis of H_2O_2. *J. Am. Chem. Soc.* **2023**, *145* (8), 4384.

(5) (a) Yamanaka, I.; Onizawa, T.; Takenaka, S.; Otsuka, K. Direct and Continuous Production of Hydrogen Peroxide with 93% Selectivity Using a Fuel-Cell System. *Angew. Chem., Int. Ed.* **2003**, *42*, 3653. (b) Xia, C.; Xia, Y.; Zhu, P.; Fan, L.; Wang, H. Direct electrosynthesis of pure aqueous H_2O_2 solutions up to 20% by weight using a solid electrolyte. *Science.* **2019**, *366*, 226. (c) Ledendecker, M.; Pizzutilo, E.; Malta, G.; Fortunato, G. V.; Mayrhofer, K. J. J.; Hutchings, G. J.; Freakley, S. J. Isolated Pd Sites as Selective Catalysts for Electrochemical and Direct Hydrogen Peroxide Synthesis. *ACS Catal.* **2020**, *10* (10), 5928.

(6) Tse, E. C. M.; Barile, C. J.; Kirchschlager, N. A.; Li, Y.; Gewargis, J. P.; Zimmerman, S. C.; Hosseini, A.; Gewirth, A. A. Proton transfer dynamics control the mechanism of O2 reduction by a non-precious metal electrocatalyst. *Nat. Mater.* **2016**, *15*, 754.

(7) (a) Wang, Y.-H.; Mondal, B.; Stahl, S. S. Molecular Cobalt Catalysts for O_2 Reduction to H_2O_2: Benchmarking Catalyst Performance via Rate-Overpotential Correlations. *ACS Catal.* **2020**, *10* (20), 12031. (b) Rana, A.; Lee, Y.-M.; Li, X.; Cao, R.; Fukuzumi, S.; Nam, W. Highly Efficient Catalytic Two-Electron Two-Proton Reduction of Dioxygen to Hydrogen Peroxide with a Cobalt Corrole Complex. *ACS Catal.* **2021**, *11* (5), 3073.

(8) (a) Chen, Z.; Concepcion, J. J.; Hull, J. F.; Hoertz, P. G.; Meyer, T. J. Catalytic water oxidation on derivatized nanoITO. *Dalton Trans.* **2010**, *39*, 6950. (b) Chen, Z.; Concepcion, J. J.; Hu, X.; Yang, W.; Hoertz, P. G. A.; Meyer, T. J. Concerted O atom-proton transfer in the O-O bond forming step in water oxidation. *Proc. Natl. Acad. Sci. U.S.A.* **2010**, *107*, 7225.

(9) (a) Chen, Z.; Concepcion, J. J.; Luo, H.; Hull, J. F.; Paul, A.; Meyer, T. J. Nonaqueous Catalytic Water Oxidation. *J. Am. Chem. Soc.* **2010**, *132*, 17670. (b) Hidalgo-Acosta, J. C.; Mendez, M. A.; Scanlon, M. D.; Vrubel, H.; Amstutz, V.; Adamiak, W.; Opallo, M.; Girault, H. H. Catalysis of water oxidation in acetonitrile by iridium oxide nanoparticles. *Chem. Sci.* **2015**, *6*, 1761.

(10) (a) Mirzakulova, E.; Khatmullin, R.; Walpita, J.; Corrigan, T.; Vargas-Barbosa, N. M.; Vyas, S.; Oottikkal, S.; Manzer, S. F.; Hadad, C. M.; Glusac, K. D. Electrode-assisted water oxidation by a flavin derivative. *Nat. Chem.* **2012**, *3*, 794−801. (b) Fisher, K. J.; Materna, K. L.; Mercado, B. Q.; Crabtree, R. H.; Brudvig, G. W. Electrocatalytic Water Oxidation by a Copper(II) Complex of an Oxidation-Resistant Ligand. *ACS Catal.* **2017**, *7*, 3384. (c) Hsu, W.-C.; Wang, Y.-H. Homogenous Water Oxidation Catalyzed by First Row Transition Metal Complexes: Unveiling the Relationship between Turnover Frequency and Reaction Overpotential. *ChemSusChem.* **2022**, *15*, No. e202102378.

(11) (a) Brunschwig, B. S.; Chou, M. H.; Creutz, C.; Ghosh, P.; Sutin, N. Mechanisms of Water Oxidation to Oxygen: Cobalt(IV) as an Intermediate in the Aquocobalt(II)-Catalyzed Reaction. *J. Am. Chem. Soc.* **1983**, *105*, 4833. (b) Dogutan, D. K.; McGuire, R.; Nocera, D. G. Electrocatalytic Water Oxidation by Cobalt (III) Hangman β-Octafluoro Corroles. *J. Am. Chem. Soc.* **2011**, *133*, 9178. (c) McCool, N. S.; Robinson, D. M.; Sheats, J. E.; Dismukes, G. C. A Co4O4 "Cubane" Water Oxidation Catalyst Inspired by Photosynthesis. *J. Am. Chem. Soc.* **2011**, *133*, 11446. (d) Wang, D.; Groves, J. T. Efficient water oxidation catalyzed by homogeneous cationic cobalt porphyrins with critical roles for the buffer base. *Proc. Natl. Acad. Sci. U.S.A.* **2013**, *110*, 15579. (e) Ishizuka, T.; Watanabe, A.; Kotani, H.; Hong, D.; Staonaka, K.; Wada, T.; Shiota, Y.; Yoshizawa, K.; Ohara, K.; Yamaguchi, K.; Kato, S.; Fukuzumi, S.; Kojima, T. Homogenous Photocatalytic Water Oxidation with a Dinuclear CoIII-Pyridylmethylamine Complex. *Inorg. Chem.* **2016**, *55*, 1154. (f) Khosrowabadi Kotyk, J. F.; Hanna, C. M.; Combs, R. L.; Ziller, J. W.; Yang, J. Y. Intramolecular hydrogen-bonding in a cobalt aqua complex and electrochemical water oxidation activity. *Chem. Sci.* **2018**, *9*, 2750. (g) Du, H.-Y.; Chen, S.-C.; Su, X.-J.; Jiao, L.; Zhang, M.-T. Redox-Active Ligand Assisted Multielectron Catalysis: A Case of CoIII Complex as Water Oxidation Catalyst. *J. Am. Chem. Soc.* **2018**, *140* (4), 1557. (h) Biswas, S.; Bose, S.; Debgupta, D.; Das, P.; Biswas, A. N. Redox-active ligand assisted electrocatalytic water oxidation by a mononuclear cobalt complex. *Dalton Trans* **2020**, *49*, 7155. (i) Bera, M.; Kaur, S.; Keshari, K.; Moonshiram, D.; Parja, S. Characterization of Reaction Intermediates Involved in the Water Oxidation Reaction of a Molecular Cobalt Complex. *Inorg. Chem.* **2022**, *61* (51), 21035.

(12) Shi, X.; Back, S.; Gill, T. M.; Siahrostami, S.; Zheng, X. Electrochemical Synthesis of H_2O_2 by Two-Electron Water Oxidation Reaction Review. *Chem.* **2021**, *7*, 38.

(13) (a) Kuttassery, F.; Sagawa, S.; Mathew, S.; Sagawa, S.; Remello, S. N.; Thomas, A.; Yamamoto, D.; Onuki, S.; Nabetani, Y.; Tachibana, H.; Inoue, H. One Electron-Initiated Two-Electron Oxidation of Water by Aluminum Porphyrins with Earth's Most Abundant Metal. *ChemSusChem.* **2017**, *10*, 1909. (b) Han, Z.; Horak, K. T.; Lee, H. B.; Agapie, T. Tetranuclear Manganese Models of the OEC Displaying Hydrogen Bonding Interactions: Application to Electrocatalytic Water Oxidation to Hydrogen Peroxide. *J. Am. Chem. Soc.* **2017**, *139*, 9108. (c) Deutscher, J.; Corona, T.; Warm, K.; Engelmann, X.; Sobottka, S.; Braun-Cula, B.; Sarkar, B.; Ray, K. Water Oxidation Reaction Mediated by an Octanuclear Iron-Oxo Cluster. *Eur. J. Inorg. Chem.* **2018**, *2018*, 4925. (d) Kuttassery, F.; Sagawa, S.; Mathew, S.; Nabetani, Y.; Iwase, A.; Kudo, A.; Tachibana, H.; Inoue,

H. Water Splitting on Aluminum Porphyrins To Form Hydrogen and Hydrogen Peroxide by One Photon of Visible Light. *ACS Appl. Energy Mater.* **2019**, *2*, 8045. (e) Ohsaki, Y.; Thomas, A.; Kuttassery, F.; Mathew, S.; Remello, S. N.; Shimada, T.; Ishida, T.; Takagi, S.; Tachibana, H.; Inoue, H. Two-electron oxidation of water to form hydrogen peroxide initiated by one-electron oxidation of Tin (IV)-porphyrins. *Journal of Photochemistry & Photobiology A: Chemistry* **2020**, *401*, No. 112732.23. (f) Mavrikis, S.; Goltz, M.; Perry, S. C.; Bogdan, F.; Leung, P. K.; Rosiwal, S.; Wang, L.; Ponce de Leon, C. Effective Hydrogen Peroxide Production from Electrochemical Water Oxidation. *ACS Energy Lett.* **2021**, *6*, 2369. (g) Mavrikis, S.; Perry, S. C.; Leung, P. K.; Wang, L.; Ponce de Leon, C. Recent Advances in Electrochemical Water Oxidation to Produce Hydrogen Peroxide: A Mechanistic Perspective. *ACS Sustainable Chem. Eng.* **2021**, *9*, 76.

(14) (a) Hong, Y. H.; Han, J. W.; Jung, J.; Nakagawa, T.; Lee, Y.-M.; Nam, W.; Fukuzumi, S. Photocatalytic Oxygenation Reactions with a Cobalt Porphyrin Complex Using Water as an Oxygen Source and Dioxygen as an Oxidant. *J. Am. Chem. Soc.* **2019**, *141* (23), 9155. (b) Mondal, B.; Chattopadhyay, S.; Dey, S.; Mahammed, A.; Mittra, K.; Rana, A.; Gross, Z.; Dey, A. Elucidation of Factors That Govern the 2e-/2H+ vs. 4e-/4H+ Selectivity of Water Oxidation by a Cobalt Corrole. *J. Am. Chem. Soc.* **2020**, *142* (50), 21040. (c) Vaillard, V. A.; Nieres, P. D.; Vaillard, S. E.; Doctorovich, F.; Sarkar, B.; Neuman, N. I. Cobalt, Iron, and Manganese Metallocorroles in Catalytic Oxidation of Water. An Overview of the Synthesis, Selected Redox and Electronic Properties, and Catalytic Activities. *Eur. J. Inorg. Chem.* **2022**, No. e202100767.

(15) (a) Chang, M.-C.; McNeece, A. J.; Hill, E. A.; Filatov, A. S.; Anderson, J. S. Ligand-Based Storage of Protons and Electrons in Dihydrozonopyrrole Complexes of Nickel. *Chem. - Eur. J.* **2018**, *24*, 8001. (b) Chang, M.-C.; Jesse, K. A.; Filatov, A. S.; Anderson, J. S. Reversible Homolytic Activation of Water via Metal-Ligand Cooperativity in a T-shaped Ni(II) Complex. *Chem. Sci.* **2019**, *10*, 1360. (c) McNeece, A. J.; Jesse, K. A.; Xie, J.; Filatov, A. S.; Anderson, J. S. Generation and Oxidative Reactivity of a Ni(II) Superoxo Complex via Ligand-Based Redox Non-Innocence. *J. Am. Chem. Soc.* **2020**, *142*, 10824. (d) McNeece, A. J.; Jesse, K. A.; Filatov, A. S.; Schneider, J. E.; Anderson, J. S. Catalytic hydrogenation enabled by ligand-based storage of hydrogen. *Chem. Commun.* **2021**, *57*, 3869. (e) Jesse, K. A.; Anferov, S. W.; Collins, K. A.; Valdez-Moriera, J. A.; Czaikowski, M. E.; Filatov, A. S.; Anderson, J. S. Direct Aerobic Generation of a Ferric Hydroperoxo Intermediate Via a Preorganized Secondary Coordination Sphere. *J. Am. Chem. Soc.* **2021**, *143*, 18121. (f) Anferov, S. W.; Filatov, A. S.; Anderson, J. S. Cobalt-Catalyzed Hydrogenation Reactions Enabled by Ligand-Based Storage of Dihydrogen. *ACS Catal.* **2022**, *12* (16), 9933. (g) Czaikowski, M. E.; McNeece, A. J.; Boyn, J.-N.; Jesse, K. A.; Anferov, S. W.; Filatov, A. S.; Mazziotti, D. A.; Anderson, J. S. Generation and Aerobic Oxidative Catalysis of a Cu(II) Superoxo Complex Supported by a Redox-Active Ligand. *J. Am. Chem. Soc.* **2022**, *144* (34), 15569. (h) Anferov, S. W.; Anderson, J. S. A cobalt adduct of an N-hydroxy-piperidinium cation. *J. Coord. Chem.* **2022**, *75* (11-14), 1853−1864.

(16) (a) Yang, L.; Powell, D. R.; Houser, R. P. Structural variation in copper(I) complexes with pyridylmethylamide ligands: structural analysis with a new four-coordinate geometry index, τ4. *Dalton Trans.* **2007**, *9*, 955. (b) Okuniewski, A.; Rosiak, D.; Chojnacki, J.; Becker, B. Coordination polymers and molecular structures among complexes of mercury(II) halides with selected 1-benzoylthioureas. *Polyhedron.* **2015**, *90*, 47.

(17) Brookhart, M.; Green, M. L. H.; Parkin, G. Agostic interactions in transition metal compounds. *Proc. Natl. Acad. Sci. U.S.A.* **2007**, *104* (17), 6908.

(18) Żamojć, K.; Zdrowowicz, M.; Rudnicki-Velasquez, P. B.; Krzymiński, K.; Zaborowski, B.; Niedziałkowski, P.; Jacewicz, D.; Chmurzyński, L. The development of 1,3-diphenylisobenzofuran as a highly selective probe for the detection and quantitative determination of hydrogen peroxide. *Free Radical Res.* **2017**, *51*, 38.

(19) Das, P. K.; Samanta, S.; McQuarters, A. B.; Lehnert, N.; Dey, A. Valence tautomerism in synthetic models of cytochrome P450. *Proc. Natl. Acad. Sci. U.S.A.* **2016**, *113* (24), 6611−6616.

(20) Espenson, J. H. *Chemical Kinetics and Reaction Mechanisms*; Mcgraw-Hill Custom Publishing: New York Etc., 1981.

(21) Laus, G. Kinetics of acetonitrile-assisted oxidation of tertiary amines by hydrogen peroxide. *J. Chem. Soc., Perkin Trans.* **2001**, *2*, 864.

(22) Wickramasinghe, L. A.; Sharp, P. R. Dihydrogen Trioxide (HOOOH) Photoelimination from a Platinum(IV) Hydroperoxo-Hydroxo Complex. *J. Am. Chem. Soc.* **2014**, *136* (40), 13979.

(23) Rountree, E. S.; McCarthy, B. D.; Eisenhart, T. T.; Dempsey, J. L. Evaluation of Homogeneous Electrocatalysts by Cyclic Voltammetry. *Inorg. Chem.* **2014**, *53*, 9983−10002.

(24) Wang, M.; Qiu, S.; Yang, H.; Huang, Y.; Dai, L.; Zhang, B.; Zou, J. Spectrophotometric determination of hydrogen peroxide in water with peroxidase-catalyzed oxidation of potassium iodide and its applications to hydroxylamine-involved Fenton and Fenton-like systems. *Chemosphere* **2021**, *270*, No. 129448.

(25) Wang, J.-W.; Sahoo, P.; Lu, T.-B. Reinvestigation of Water Oxidation Catalyzed by a Dinuclear Cobalt Polypyridine Complex: Identification of CoO_x as a Real Heterogenous Catalyst. *ACS Catal.* **2016**, *6*, 5062.

(26) Gerken, J. B.; McAlpin, J. G.; Chen, J. Y. C.; Rigsby, M. L.; Casey, W. H.; Britt, R. D.; Stahl, S. S. Electrochemical Water Oxidation with Cobalt-Based Electrocatalysts from pH 0−14: The Thermodynamic Basis for Catalyst Structure, Stability, and Activity. *J. Am. Chem. Soc.* **2011**, *133* (36), 14431.

(27) Jenkins, D. M.; Peters, J. C. Spin-State Tuning at Pseudotetrahedral d7 Ions: Examining the Structural and Magnetic Phenomena of Four-Coordinate [BP3]CoII−X Systems. *J. Am. Chem. Soc.* **2005**, *127* (19), 7148−7165.

(28) Jessup, W.; Dean, R. T.; Gebicki, J. M. Iodometric determination of hydroperoxides in lipids and proteins. *Methods Enzymol.* **1994**, *233*, 289.